Mon. Not. R. Astron. Soc. **000**, 1–8 (2013) Printed 20 August 2014 (MN LATEX style file v2.2)

GRB 140206A: the most distant polarized Gamma-Ray Burst

D. Götz[1⋆], P. Laurent[2], S. Antier[1], S. Covino[3], P. D'Avanzo[3], V. D'Elia[4,5], A. Melandri[3]

[1] *AIM (UMR 7158 CEA/DSM-CNRS-Université Paris Diderot) Irfu/Service d'Astrophysique, Saclay, F-91191 Gif-sur-Yvette Cedex, France*
[2] *APC (UMR 7164 CEA/DSM/Irfu, Université Paris Diderot, CNRS/IN2P3, Observatoire de Paris) 10, rue Alice Domon et Léonie Duquet, 75205 Paris Cedex 13, France*
[3] *INAF – Osservatorio Astronomico di Brera, Via E. Bianchi 46, 23807 Merate (LC), Italy*
[4] *INAF-Osservatorio Astronomico di Roma, Via Frascati 33, I-00040 Monteporzio Catone, Italy*
[5] *ASI-Science Data Center, Via del Politecnico snc, I-00133 Rome, Italy*

arXiv:1408.4121v1 [astro-ph.HE] 18 Aug 2014

Accepted . Received ; in original form

ABSTRACT

The nature of the prompt γ-ray emission of Gamma-Ray Bursts (GRBs) is still far from being completely elucidated. The measure of linear polarization is a powerful tool that can be used to put further constraints on the content and magnetization of the GRB relativistic outflows, as well as on the radiation processes at work.

To date only a handful of polarization measurements are available for the prompt emission of GRBs. Here we present the analysis of the prompt emission of GRB 140206A, obtained with *INTEGRAL*/IBIS, *Swift*/BAT, and *Fermi*/GBM. Using *INTEGRAL*/IBIS as a Compton polarimeter we were able to constrain the linear polarization level of the second peak of this GRB as being larger than 28% at 90% c.l.

We also present the GRB afterglow optical spectroscopy obtained at the Telescopio Nazionale Galileo (TNG), which allowed us the measure the distance of this GRB, z=2.739. This distance value together with the polarization measure obtained with IBIS, allowed us to derive the deepest and most reliable limit to date ($\xi < 1\times10^{-16}$) on the possibility of Lorentz Invariance Violation, measured through the vacuum birefringence effect on a cosmological source.

Key words: gamma-rays burst: general – gamma-rays burst: individual: GRB 140206A – polarization – gravitation

1 INTRODUCTION

Gamma-Ray Bursts (GRBs) are transient sources whose duration spans from ms up to thousands of seconds in some cases. Most of their energy is emitted in the γ-ray band around a few hundreds of keV and they appear unpredictably at random directions on the whole sky, making their understanding challenging. In fact, despite the recent progresses in the GRB field, mainly obtained thanks to GRB-dedicated instrumentation, like the one on the *Swift* and *Fermi* satellites (see e.g. Gehrels et al. 2009; Zhang 2014), the nature of the prompt emission of GRBs is still not completely clear. On the other hand, much information could be obtained from the long-lived GRB afterglows in the X-ray, optical, and radio bands. GRBs have been proven to be of cosmological origin, with their redshifts, z, distributed in the range $[0.1, \sim 9]$, and several of them are now firmly associated with Supernovae of type Ib/c, and hence with the collapse of massive stars.

GRBs emit during a few seconds a huge amount of isotropic equivalent energy, $E_{\rm iso}$, that spans from 10^{50} to 10^{54} erg (e.g. Amati 2008), making them the most luminous events in the Universe, temporarily outshining all other sources. However, GRBs are likely collimated sources and the true emitted energy is then reduced to about 10^{51} erg (Frail et al. 2001; Bloom et al. 2003; Ghirlanda et al. 2012). Nonetheless, the exact geometry and content of this collimated jet, as well as its magnetization are not elucidated yet, and the details of the mechanism leading to the γ-ray emission are still not completely clear. Models include unmagnetized fireballs, where the observed emission could be produced by relativistic ($\Gamma \gtrsim 100$) electrons accelerated

⋆ E-mail: diego.gotz@cea.fr

in internal shocks propagating within the outflow (Rees & Mészáros 1994), and span to pure electromagnetic outflows where the radiated energy comes from magnetic dissipation (Lyutikov 2006). Intermediate cases with mildly magnetized outflows are also envisaged (e.g. Spruit et al. 2001).

Polarization measurements could add an additional constraint with respect to spectral and timing information, and indeed in the recent years, some measurements of polarization during the prompt emission of GRBs in the hundreds of keV energy range have been attempted using *INTEGRAL*/IBIS, *INTEGRAL*/SPI, and IKAROS/GAP (Kalemci et al. 2007; McGlynn et al. 2007, 2009; Götz et al. 2009, 2013; Yonetoku et al. 2011, 2012). Thanks to these measurements the open questions mentioned above could be tackled. In fact, even if globally incoherent, in the case where the magnetic field is mainly transverse and locally highly ordered, i.e. has a local coherence scale which is larger than the typical size $\sim R/\Gamma$ of the visible part of the emitting region, a synchrotron polarized signal can still be detected. This scenario has been favoured in the case of GRB 041219A (Götz et al. 2009), where a time resolved analysis could be performed, and the rapid polarization angle variations could be explained by the variation of the bulk Lorentz factors Γ of the emission regions. On the other hand, for GRBs for which just a time integrated measure is available, different scenari like the case of a random field or an ordered magnetic field parallel to the expansion velocity, for which the polarization of the detected signal should vanish, except for the peculiar condition of a jet observed slightly off-axis (e.g. Lazzati et al. 2004), cannot be completely excluded.

Further clues on the magnetic structure of GRB jets, but at later times with respect to the prompt emission, came recently thanks to the results presented by Mundell et al. (2013). They report the detection of a high level of linear polarization (28±4%) in the early optical afterglow of GRB 120308A, indicating the presence of large scale magnetic field surviving long after the initial explosion. In that case the emission has been modelled as due mainly to the reverse shock taking place when the relativistic ejecta interact with the GRB ambient medium. Indeed the GRB early afterglow emission is produced by a combination of the radiation of the forward and reverse shock, and the reverse shock tests the magnetic structure of the inner part of the jet, just like prompt emission, but at slightly later times, when the prompt emission produced internally to the jet is over.

Finally we note that polarization measures in cosmological sources are also a valuable tool for fundamental physics experiments: Lorentz Invariance Violation (LIV) arising from the phenomenon of vacuum birefringence can be constrained as recently shown by Fan et al. (2007), Laurent et al. (2011a), Stecker (2011), Toma et al. (2012), and Götz et al. (2013).

Here we present the prompt emission analysis of GRB 140206A obtained with *INTEGRAL*, *Swift*, and *Fermi*/GBM, as well as its polarization measurements obtained with *INTEGRAL* (section 2). We also present the spectroscopy of the GRB afterglow obtained with the Telescopio Nazionale Galileo (TNG) (section 3) and discuss our results, including the LIV limits (section 4) we can obtain from this GRB, in section 5.

2 DATA ANALYSIS AND RESULTS

GRB 140206A has been detected by the *INTEGRAL* Burst Alert System (IBAS; Mereghetti et al. 2003) on February 2^{nd} 2014, and localized to R.A. = $09^h41^m13.03^s$ Dec.= $+66^\circ45'54.7''$, with an 90% c.l. uncertainty of $0.8'$ (Götz et al. 2014). The burst has been also been detected and localized by *Swift* (Lien et al. 2014) and the GBM on board *Fermi* (von Kienlin et al. 2014). A bright optical afterglow at a position consistent with the prompt one, peaking at about the 15^{th} magnitude was reported by several telescopes (Oksanen et al. 2014; Oates et al. 2014; Yurkov et al. 2014; Xu et al. 2014; Volnova et al. 2014; Sonbas et al. 2014; D'Avanzo et al. 2014; Masi et al. 2014; Saito et al. 2014; Kopac et al. 2014; Quadri et al. 2014; Toy et al. 2014). The brightness of the optical counterpart allowed to measure the redshift of the GRB ($z \sim 2.7$) independently by two groups (Malesani et al. 2014; D'Elia et al. 2014). In the following sections we present the analysis of the prompt γ-ray emission of GRB 140206A and of its optical afterglow.

2.1 IBIS/ISGRI

IBIS (Ubertini et al. 2003) is a coded mask telescope on board the *INTEGRAL* satellite (Winkler et al. 2003). It is made by two superposed pixellated detector layers, ISGRI (Lebrun et al. 2003) working in the 15 keV–1 MeV energy range, and PICsIT (Di Cocco et al. 2003), working in the 200 keV – 10 MeV energy range. Here we restrict our analysis to the ISGRI detector plane. Indeed, due to satellite telemetry limitations, PICsIT spectral–imaging data are temporally binned over the entire duration of an *INTEGRAL* pointing (typically 30-45 minutes) and hence they are not suited for studies of GRBs, while for PICsIT spectral–timing data no proper response matrix is available yet.

GRB 140206A has been detected by IBIS/ISGRI at the very beginning of the *INTEGRAL* orbit, while still close to the radiation belts. So, due to the high count rate induced by the residual particle flux, not all the data could be transmitted to the ground, especially while the GRB was at its peak. This is why we decided to include in this paper also the *Swift* and *Fermi*/GBM data analysis in order to have a complete picture of the GRB. Otherwise e.g. the GRB peak flux and fluence would have been underestimated.

Using the *INTEGRAL* Off-line Scientific Analysis (OSA) software v. 10.0 we extracted the ISGRI light curve of GRB 140206A in 3 s time bins, which is the shortest time bin for which sufficient data are available. As can be seen from Fig. 1, most of the time bins are empty due to the telemetry loss. Nevertheless due to the high flux of the GRB the time bins for which an analysis is possible have rather high statistics reaching up to 2500 counts/bin. This allowed us to extract two spectra, corresponding to the two main peaks of the GRB, namely from 07:17:20.0 to 07:17:50.0 U.T. for the first peak and from 07:18:10.0 to 07:18:40 U.T. for the second peak. These spectra have been used for the common spectral fit with the other instruments, see below.

We note that telemetry bandwidth limitations do not affect the polarimetric results (see below), since Compton events packets are prioritized in the IBIS telemetry transmission.

2.2 Swift/BAT

The *Swift*/BAT (Gehrels et al. 2004; Barthelmy et al. 2005) data have been downloaded through the *Swift* public archive[1], and analysed with the tools provided by HEASARC v. 6.15.1, and the latest version of CALDB. BAT standard products, including the light curve shown in Fig. 1, have been extracted using `batgrbproduct`. Previously, the mask weightening which produces background-subtracted lights curves and spectrum has been validated using `fkeyprint`. The detector quality map of the two peaks has been computed taking into account the same time intervals as for ISGRI, with the help of `batgbin` which creates a detector plane image, and `batdetmask`, retrieving the appropriate detector quality map from CALDB. The two spectra of the two main peaks, have been derived using `batbinevt` and several corrections needed to fit the two spectrum with `xspec` (see Section 2.4) have been applied using `batupdatephakw` and `batphasyserr`. The appropriate response matrices have been derived using `batdrmgen`. The BAT data have been used to measure the GRB T_{90} duration resulting to be 93.2±13.5 s in the 15–300 keV energy band.

2.3 GBM

Fermi/GBM (Meegan et al. 2009) data have been obtained through the *Fermi* SSC[2], and analysed using the RMFIT v. 432 package[3]. Using the quick look data, we chose the NaI and BGO detectors for which the GRB signal is stronger. This corresponds to the NaI detectors number 8 and 11, and to the BGO number 1. The light curves of the three detectors have been computed by subtracting the background fitted using a fourth degree polynomial function over time intervals before and after the GRB, excluding the GRB itself.

As can be seen from Fig. 1, only the second peak of the GRB has been detected in the GBM data, because of the occultation of the source by the Earth during the first peak. A spectrum of the second peak has been extracted for the three detectors mentioned above, using again the same time interval as for ISGRI. The spectra have been exported to PHA format, and the latest available response matrices have been obtained through the CALDB database.

2.4 Joint Spectral Analysis

BAT provides the most complete data set for GRB 140206A. That is why we used these data to derive the GRB peak flux and fluence. The GRB peak flux in the 15–350 keV energy band measured over 1 s is 20.7±1.0 ph cm^{-2}. The GRB fluence measured over the entire burst duration is about 2×10^{-5} erg cm^{-2}. The average BAT spectrum is well fitted (χ^2/d.o.f.=64.7/72) by a power law with an exponential high-energy cut-off, with a photon index Γ=1.1±0.15 and a cut-off energy E_c=114^{+47}_{-26} keV. The errors are reported at 90% c.l.

The spectra of the two peaks derived for the different instruments (see above), have been fitted simultaneously using

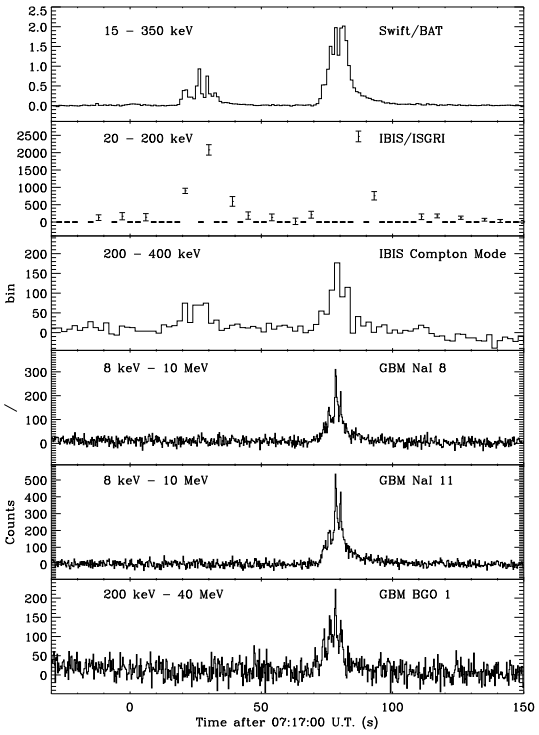

Figure 1. Light curves of GRB 140206A as seen by different detectors. The detector name and energy range are reported in each panel. Note that except for BAT for which the counts are reported per detector pixel, the global count rate for each instrument is shown. The time bin is 1 s for BAT, 3 s for IBIS/ISGRI, 2 s for IBIS Compton Mode and 0.25 s for the GBM detectors. The first peak of the GRB is missing in the GRB data due to Earth occultation.

`xspec` v. 12.7.0 (Arnaud 1996). For the first peak only ISGRI and BAT spectra have been used. A constant multiplicative factor has added in order to account for cross-calibration uncertainties and ISGRI data loss. For the joint fit of the first peak, see Fig. 2, a simple power law could be excluded (χ^2/d.o.f.=133.3/109), and a cut-off power law represented a better model for the data (χ^2/d.o.f.=112/108). A fit using a Band function (Band et al. 1993) did not increase further the quality of the fit (χ^2/d.o.f.=112/107).

For the second peak we used BAT, ISGRI, and GBM BGO data. GBM NaI data have been excluded due to their lower statistical quality with respect to ISGRI and BAT. In this case, thanks to the BGO data extending the spectral coverage to higher energies, the best fit model is represented by a Band model (χ^2/d.o.f.=148/121), since the fits using a single power law (χ^2/d.o.f.=465/123) or a cut-off power law (χ^2/d.o.f.=162/122) turn out to be less adapted to the data. The spectral fitting results for both peaks are reported in Table 1. One can see that the GRB peak energy, E_p, decreases with time, and that both values are on the soft end of the peak energy distribution of the GRBs observed with *INTEGRAL*, *Fermi*/GBM or BATSE (Bošnjak et al. 2014).

[1] http://swift.gsfc.nasa.gov
[2] http://fermi.gsfc.nasa.gov/ssc/
[3] http://fermi.gsfc.nasa.gov/ssc/data/analysis/rmfit/

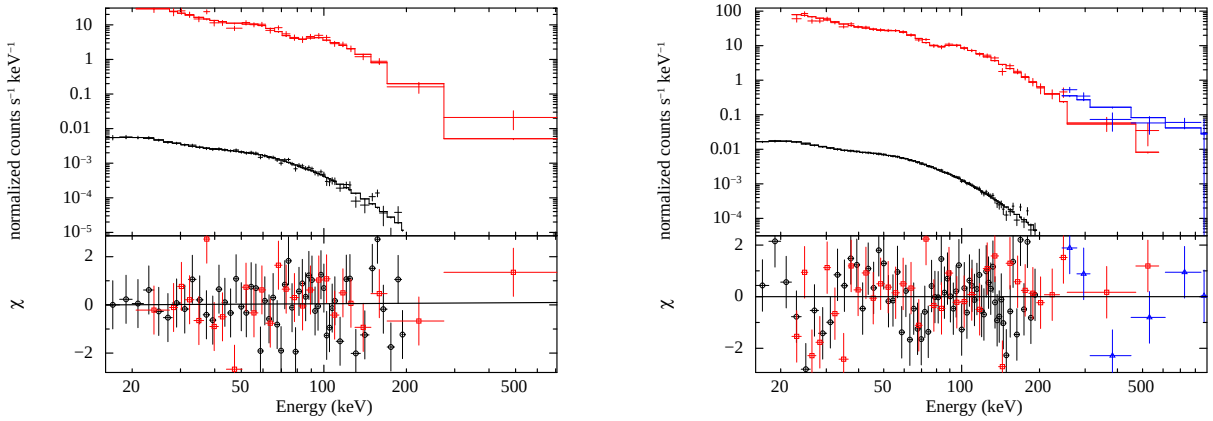

Figure 2. Left: Joint Swift/BAT (black) and IBIS/ISGRI (red) spectrum of the first peak of GRB 140206A. The upper panel shows the recorded counts and the best fit model, while the lower panel shows the residuals with respect to the model using circles for BAT and squares for ISGRI. Right: Joint Swift/BAT (black), IBIS/ISGRI (red), GBM/BGO (blue) spectrum of the second peak of GRB 140206A. The upper panel shows the recorded counts and the best fit model, while the lower panel shows the residuals with respect to the model using circles for BAT, squares for ISGRI, and triangles for the BGO.

Table 1. Spectral fitting results for GRB 140206A. Errors are given at 90% c.l.

First Peak			
Photon Index Γ	Cut-off energy E_c	–	E_p
1.13±0.16	150^{+92}_{-44} keV	–	130^{+80}_{-38} keV
Second Peak			
α	E_0	β	E_p
0.94±0.08	92±16 keV	$2.0^{+0.2}_{-0.3}$	98±17 keV

2.5 Polarization

The two superposed pixellated detector layers permit to IBIS to be used as a Compton telescope by measuring the properties of the photons (time, energy and position) interacting in both planes. Thanks to the polarization dependency of the differential cross section for Compton scattering, linearly polarized photons scatter preferentially perpendicularly to the incident polarization vector. Hence a Compton telescope can be used also as a polarimeter, and IBIS allowed us to date to detect polarization in five different bright objects, the Crab nebula (Forot et al. 2008), the black hole binary Cyg X–1 (Laurent et al. 2011b), GRB 041219A (Götz et al. 2009), GRB 061122 (Götz et al. 2013), and GRB 120711A (Martin-Carrillo et al., in prep.). In this work we adopt the same analysis technique as described in these references.

Due to the nature of Compton scattering, one can expect an azimuthal distribution of the scattered photons on the telescope lower plane of the form

$$N(\phi) = S[1 + a_0 \cos 2(\phi - \phi_0)], \quad (1)$$

where S is the average source flux, a_0 is the flux amplitude modulation, ϕ the azimuthal scattering angle, $P.A. = \phi_0 - \pi/2 + n\pi$ is the polarization angle (where 0° corresponds to the North and 90° to the East). The polarization fraction is defined as $\Pi = a_0/a_{100}$, where a_{100} is the amplitude expected for a 100% polarized source derived by Monte Carlo simulations of the instrument (see e.g. Forot et al. 2008).

In Fig. 1 we report the IBIS background-subtracted light curve of GRB 140206A, derived using the Compton mode events in the 200–400 keV energy range. Due to the softness of the event, no signal has been detected above those energies.

We performed the polarization analysis over different time intervals of the GRB. The best signal-to-noise ratio is obtained over the 07:18:10.0–07:18:30.0 U.T. time interval (corresponding to the second peak, Compton image SNR=13.5). As can be seen from Fig. 1, the GRB first peak has not enough statistics to perform a sensitive analysis. In order to compute a_{100}, we used the spectral analysis described above. Using these spectral parameters, a_{100} has been computed through Monte Carlo simulations, and turns out to be 0.29±0.03 (68% c.l.).

Following the method reported in Götz et al. (2013) we first built the source polarigram (i.e. source flux as a function of ϕ) in the 200–400 keV energy band, see Fig. 3. We then divided the selected time interval in smaller energy intervals (200–250 keV; 250–300 keV; 300–400 keV), but only the first energy interval provides a sufficiently high detection level in order to constrain polarization (SNR=10.6). We fitted the polarigrams with Eq. 1 using a least squares technique (χ^2/d.o.f.=2.31/2) to derive a_0 and ϕ_0, see Fig. 3. Confidence intervals on a_0 and ϕ_0 were, on the other hand, not derived from the fit, since the two variables are not independent. They were derived from the probability density distribution of measuring a and ϕ from N independent data points over a π period, based on Gaussian distributions for the orthogonal Stokes components (see Eq. 2 in Forot et al. 2008).

Over the selected time interval we measure a high polarization level in the 200–400 keV energy band, deriving a 68% c.l. lower limit to the polarization fraction (Π) of 48%

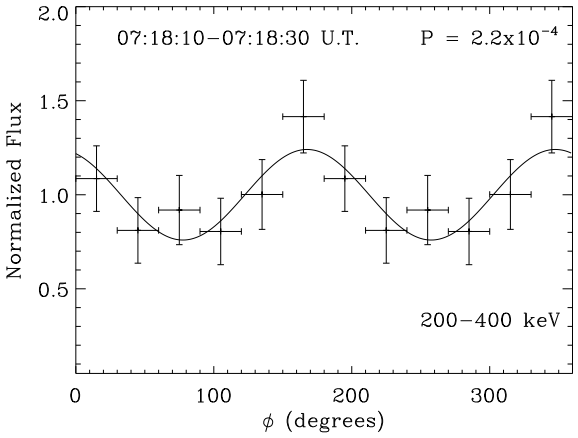

Figure 3. Polarigram of GRB 140206A in the 200–400 keV energy band. The crosses represent the data points (replicated once for clarity) and the continuous line the fit done on the first 6 points using Eq. 1. The chance probability P of a non-polarized (<1%) signal is also reported. The normalized flux corresponds to $N(\phi)/S$

.

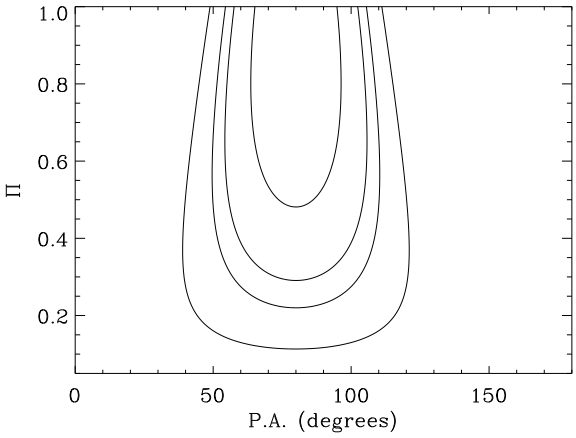

Figure 4. The 68%, 90%, 95%, and 99% (top to bottom) confidence contours for the Π and *P.A.* parameters.

Table 2. Polarization measurements of GRB 140206A.

Energy band (keV)	Π (%) (68% c.l.)	P.A. (°) (68% c.l.)	Π (%) (90% c.l.)	P.A. (°) (90% c.l.)
200–400	>48	80±15	>28	80±25

and the corresponding polarization angle (*P.A.*) is 80±15°, see Table 2. The 68%, 90%, 95%, and 99% confidence regions for the two parameters are shown in Fig. 4, where one can see that the 95% c.l. lower limit to Π is 25%. For each polarigram we also computed the probability, P, the source we measure corresponds to an un-polarized (Π <1%) source. This value is reported in Fig. 3. As stated above, the same analysis has been performed in different energy bands, but only the 200–250 keV energy band shows an un-polarized probability of 3×10^{-4}, while the two others do not show a statistically significant detection. The derived parameters for the 200–250 keV energy band are statistically consistent with the ones of the 200–400 keV energy band.

3 TNG

The spectroscopy of GRB 140206A was carried out at the Telescopio Nazionale Galileo (TNG) using the DOLORES camera in slit mode, with the LR-B grism (D'Elia et al. 2014). This configuration covers the spectral range 3000 − 8430Å with a resolution of $\lambda/\Delta\lambda = 585$ for a slit width of 1" at the central wavelength 5850Å. The observation started at 2014-02-06T19:53:07, i.e., ∼ 12.6 hrs after the GRB, with a total exposure of 1800 s. The slit position angle was set to the parallatic value.

The spectra were extracted using standard procedures (bias and background subtraction, flat fielding, wavelength and flux calibration) under the packages ESO-MIDAS[4] and IRAF[5]. Ne-Hg and Helium lamps were used for wavelength calibration. A spectrophotometric star could not be acquired the same night of the target, so we used the normalized spectrum for our analysis.

The TNG spectrum shows several absorption lines that can be interpret as due to Ly-β, Ly-α, NV λλ1238,1242, SiII λ1260, OI λ1302, SiII λ1304, CII λ1334, SiIV λλ1393,1402, SiII λ1526, CIV λλ1548,1550, FeII λλ1608,1611, AlII λ1670, AlIII λλ1854,1862 at a common redshift of $z = 2.739 \pm 0.001$, corresponding to a luminosity distance of 23 Gpc[6], and implying an $E_{\rm iso}$ of $(2.4\pm0.2)\times10^{54}$ erg. In addition, we also detect at the same redshift faint fine structure lines from excited levels of SiII* λ1533 and FeII* λλ1618,1621. These levels are produced by the GRB light which photoexcites the intervening gas at distances in the range 0.1–2 kpc (see, e.g. Prochaska et al. 2006; Vreeswijk et al. 2007; D'Elia et al. 2009). Thus, the excited gas resides in the GRB host, confirming that the GRB is at redshift z=2.739±0.001.

Our redshift determination is in perfect agreement with the reported value by Malesani et al. (2014).

Finally, we also detect a strong intervening Ly-alpha absorber at $z = 2.32$. The TNG spectrum with all the absorption features is shown in Fig. 5.

4 LIV LIMITS

The possible unification at the Planck energy scale of the theory of General Relativity and the quantum theory in the form of the Standard Model requires to quantize gravity, which can lead to fundamental difficulties: one of these is to

[4] http://www.eso.org/projects/esomidas/
[5] http://iraf.noao.edu/
[6] Assuming H_0=71 km/s/Mpc, Ω_M=0.27, Ω_λ=0.73

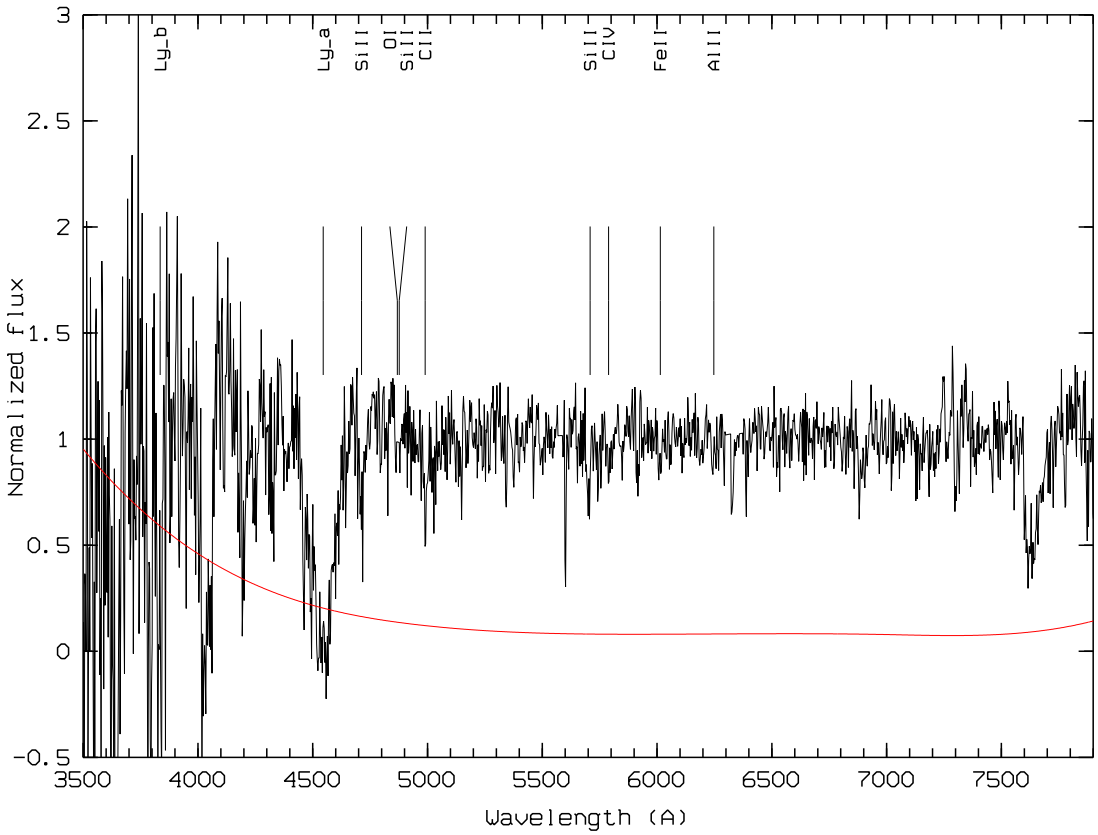

Figure 5. The TNG spectrum (black) and its error spectrum (red). Vertical lines mark the strongest absorption features. The Ly-α intervening absorber at z=2.32 is the wide feature at $\sim$ 4000 Å.

admit the Lorentz Invariance Violation (LIV) (e.g. Jacobson et al. 2006; Liberati & Maccione 2009; Mattingly 2005)

A possible experimental test for such violation is to measure the helicity dependence of the propagation velocity of photons (see e.g. Laurent et al. 2011a, and references therein). The light dispersion relation is given in this case by

$$\omega^2 = k^2 \pm \frac{2\xi k^3}{M_{Pl}} \equiv \omega_{\pm}^2 \tag{2}$$

where $E = \hbar\omega$, $p = \hbar k$, M_{Pl} is the Planck Mass, and the sign of the cubic term is determined by the chirality (or circular polarization) of the photons, which leads to a rotation of the polarization during the propagation of linearly polarized photons. This effect is known as vacuum birefringence.

Equation 2 can be approximated as follows

$$\omega_{\pm} = |k|\sqrt{1 \pm \frac{2\xi k}{M_{Pl}}} \approx |k|(1 \pm \frac{\xi k}{M_{Pl}}) \tag{3}$$

where ξ gives the order of magnitude of the effect. In practice some quantum-gravity theories (e.g. Myers & Pospelov 2003) predict that the polarization plane of the electromagnetic waves emitted by a distant source rotates by a quantity $\Delta\theta$ while the latter propagates through space, and this as a function of the energy of the photons, see Eq. 4, where d is the distance of the source:

$$\Delta\theta(p) = \frac{\omega_+(k) - \omega_-(k)}{2}\, d \approx \xi \frac{k^2 d}{2M_{Pl}} \tag{4}$$

As a consequence the signal produced by a linearly polarized source, observed in a given energy band could vanish, if the distance is large enough, since the differential rotation acting on the polarization angle as a function of energy would in the end add opposite oriented polarization vectors, and hence in a net un-polarized signal. But being this effect very tiny, since it is inversely proportional to the Planck Mass (M_{Pl} $\sim$2.4$\times$10^{18} GeV), the observed source needs to be at cosmological distances. The simple fact to detect the polarization signal from a distant source, can put a limit to such a possible violation. This experiment has been performed recently by Laurent et al. (2011a), Toma et al. (2012), and Götz et al. (2013) making use of the prompt emission of GRBs. Indeed, since GRBs are at the same time at cosmological distances, and emitting at high energies, their polarization measurements are highly suited to measure and improve upon these limits.

By taking the distance of GRB 140206A we derived

above, i.e. 23 Gpc, and if we set $\Delta\theta(k) = 90^\circ$ (the fact that we measure the polarization in a given energy band means that the differential rotation should not be grater than this value), we obtain

$$\xi < \frac{2M_{Pl}\Delta\theta(k)}{(k_2^2 - k_1^2)\ d} \approx 1 \times 10^{-16}, \quad (5)$$

improving the previous limit (Götz et al. 2013) by a factor three.

5 DISCUSSION AND CONCLUSIONS

We measured the timing and spectral properties of the prompt γ-ray emission of GRB 140206A, using *Swift*/BAT, *Fermi*/GBM, and *INTEGRAL*/IBIS. Using IBIS in Compton mode we were able to measure the linear polarization in the γ-ray energy band (200–400 keV) during the second and brightest peak of the prompt emission of GRB 140206A, putting a lower limit on the polarization level of 28% (90% c.l.). This measure, follows some recent reports of detections of high (and variable) polarization levels in the prompt emission of a few other GRBs: 041219A by Götz et al. (2009); McGlynn et al. (2007), 061122 by Götz et al. (2013); McGlynn et al. (2009), 100826A, 110301A and 110721A by Yonetoku et al. (2011, 2012), see Table 3. Although all these measures, taken individually, have not a very high significance ($\gtrsim$3 σ), they indicate that GRBs are indeed good candidates for highly γ-ray polarized sources, and that they are prime targets for future polarimetry experiments. On the other hand, as can be seen from Table 3 the currently available GRB sample does not show extreme spectral characteristics, like e.g. in terms of peak energy, but they are on the upper end of the GRB fluence distribution. This means that, on one hand, this sample may be well representative of the whole GRB population. On the other hand the fluence bias is clearly an instrumental selection effect due to the high photon statistics needed to perform the polarization measurements in IBIS and GAP.

As discussed in Götz et al. (2009, 2013) these polarization features can be explained by synchrotron radiation in an ordered magnetic field (Granot 2003; Granot & Königl 2003; Nakar et al. 2003), by the jet structure (Lazzati & Begelman 2009), or , independently from the magnetic field structure or the emission processes, by the observer's viewing angle with respect to the jet (Lazzati et al. 2004), even in the case of thermal radiation from the jet photosphere (Lundman et al. 2014). In addition the level of magnetization of the jet can also play role (Spruit et al. 2001; Lyutikov 2006). For instance the ICMART model (Zhang & Huirong 2011), which implies a magnetically dominated wind launched by the central engine, predicts a decrease of the polarization level during GRB individual pulses, but this hypothesis cannot be tested with the current data. Indeed, as pointed out by Toma et al. (2009), the different models are hardly distinguishable relaying only on γ-ray data, and a result can be achieved only on statistical grounds, i.e. having a sample of several tens of measures at high energies.

On the other hand, the recent detection of a high level (Π=28$\pm$4%) of linear optical polarization in the early afterglow of GRB 120308A, allowed Mundell et al. (2013) to point out the presence of a magnetized reverse shock with an ordered magnetic field, confirming the presence of high magnetic fields in the GRB ejecta, and indicating that the multi-wavelength approach could be more fruitful while waiting for a dedicated GRB polarimetry mission, like e.g. POLAR (Bao et al. 2012) or POET (McConnell et al. 2009).

Thanks to our TNG spectrum of the GRB afterglow, we were able to precisely measure the distance of our source, $z = 2.739$, making of GRB 140206A the most distant GRB for which IBIS was able to measure a polarized signal. Our distance measurement together with the polarization measure obtained with IBIS, allowed us to derive the deepest and most reliable limit ($\xi < 1\times10^{-16}$) to date on the possibility of Lorentz Invariance Violation, measured through the vacuum birefringence effect on a cosmological source. GRB 140206A is namely the first and only GRB for which a polarization measurement of the prompt emission and spectroscopically determined distance are available at once.

ACKNOWLEDGEMENTS

Based on observations with INTEGRAL, an ESA project with instruments and science data centre funded by ESA member states (especially the PI countries: Denmark, France, Germany, Italy, Switzerland, Spain), Czech Republic and Poland, and with the participation of Russia and the USA, and on observations made with the TNG under programme ID A26 TAC_63. ISGRI has been realized and maintained in flight by CEA-Saclay/Irfu with the support of CNES. This research has made use of data, software and/or web tools obtained from NASA's High Energy Astrophysics Science Archive Research Center (HEASARC), a service of Goddard Space Flight Center and the Smithsonian Astrophysical Observatory. We acknowledge the financial support of the UnivEarthS Labex program at Sorbonne Paris Cité (ANR-10-LABX-0023 and ANR-11-IDEX-0005-02), of ASI grant I/004/11/0 and of PRIN-MIUR 2009 grants.

REFERENCES

Amati L., Guidorzi C., Frontera F., Della Valle M., Finelli F., Landi R., Montanari E., 2008, MNRAS, 391, 577
Arnaud K. A., 1996, Astronomical Society of the Pacific Conference Series, 101, 17
Band D. et al., 1993, ApJ, 413, 281
Bao T.W. et al., 2012, SPIE, 8443
Barthelmy S. et al., 2005, Space Sci. Rev., 120, 143
Bloom J. S., Frail D. A., Kulkarni S. R., 2003, ApJ, 594, 674
Bošnjak, Ž., Götz D., Bouchet L., Schanne S., Cordier B., et al., 2014, A&A, 561, A25
McConnell, M.L. et al., 2009, AIPC, 1133, 64
D'Avanzo, P., Covino S., Melandri A., di Fabrizio L., 2014, GCN, 15799
D'Elia V. et al., 2009, ApJ, 694, 332
D'Elia V., D'Avanzo P., Covino S., Melandri A., Vergani S. D., di Fabrizio L., 2014, GCN, 15802
Di Cocco G. et al., 2003, A&A, 411, L189
Fan Y.-Z., Wei D.-M., Xu D., 2007, MNRAS, 376, 1857
Forot M., Laurent P., Grenier I.A., Gouiffès C., Lebrun F., 2008, ApJ, 688, L29

Table 3. Summary of recent GRB polarization measurement by IBIS and GAP.

GRB	Π (68% c.l.)	Peak energy (keV)	Fluence and Energy Range (erg cm^{-2})	z	Instrument
041291A	65±26%	201^{+80}_{-41}	2.5×10^{-4} in 20–200 keV	$0.31^{+0.54}_{-0.26}$	IBIS
06122	>60%	188±17	2.0×10^{-5} in 20–200 keV	$1.33^{+0.77}_{-0.76}$	IBIS
100826A	25±15%	606^{+134}_{-109}	3.0×10^{-4} in 20 keV–10 MeV	0.71–6.84[1]	GAP
110301A	70±22%	107±2	3.6×10^{-5} in 10 keV–1 MeV	0.21–1.09[1]	GAP
110721	84^{+16}_{-28}%	393^{+199}_{-104}	3.5×10^{-4} in 10 keV–1 MeV	0.45–3.12[1]	GAP
140206A	>48%	98±17	2.0×10^{-5} in 15–350 keV	2.739±0.001	IBIS

[1] redshift based on empirical prompt emission correlations, not on afterglow observations.

Frail D. A. et al., 2001, ApJ, 562, L55
Gehrels N. et al., 2004, ApJ, 611, 1005
Gehrels N., Ramirez-Ruiz E., Fox D. B., 2009, ARA&A, 47, 567
Ghirlanda G., Nava L., Ghisellini G., Celotti A., Burlon D., Covino S., Melandri A., 2012, MNRAS, 420, 483
Götz D., Laurent P., Lebrun F., Daigne F., Bošnjak Ž., 2009, ApJ, 695, L208
Götz D., Covino S., Fernández-Soto A., Laurent P., Bošnjak, Ž., 2013, MNRAS, 431, 3550
Götz D., Mereghetti S., Bozzo E., Ferrigno C., Tuerler M., Borkowski J., 2014, GCN, 15785
Granot J., 2003, ApJ, 596, L17
Granot J., Königl A., 2003, ApJ, 594, L83
Jacobson T., Liberati S., Mattingly D., 2006, Annals of Physics, 321, 150
Kalemci E., Boggs S. E., Kouveliotou C., Finger M., Baring M. G., 2007, ApJS, 169, 75
von Kienlin A., Bhat P.N., 2014, GCN, 15796
Kopac D., Gomboc A., Guidorzi C., Melandri A., Steele I.A., Mundell C., 2014, GCN 15806
Laurent P., Götz D., Binétruy P., Covino S., Fernandez-Soto A., 2011a, Phys. Rev. D, 83, 12, 121301
Laurent P., Rodriguez J., Wilms J., Cadolle Bel M., Pottschmidt K., Grinberg V., 2011b, Science, 332, 438
Lazzati D., Rossi E., Ghisellini G., Rees M.J., 2004, MNRAS, 347, L1
Lazzati D., Begelman M.C., 2009, ApJ, 700, L141
Lebrun F. et al., 2003, A&A, 411, L141
Liberati S., Maccione L., 2009, Annual Review of Nuclear and Particle Science, 59, 245
Lien A.Y. et al., 2014, GCN 15784
Lundman C., Pe'er A., Ryde F., 2014, MNRAS, 440, 3292
Lyutikov M., 2006, New Journal of Physics, 8, 199
Masi G., Nocentini, F., 2014, GCN 15801
Mattingly D., 2005, Living Reviews in Relativity, 8, 5
McGlynn S. et al., 2007, A&A, 466, 895
McGlynn S. et al., 2009, A&A, 499, 465
Meegan C. et al., 2009, ApJ, 702, 791
Mereghetti S., Götz D., Borkowski J., Walter R., Pedersen H., 2003, A&A, 411, L291
Malesani D. et al., 2014, GCN 15800
Mundell C.G. et al., 2013, Nature, 504, 119
Myers R.C., Pospelov M., 2003, Phys. Rev. Lett., 90, 211601
Nakar E., Piran T., Waxman E., 2003, JCAP, 10, 005
Oates, S. R., Lien A. Y., 2014, GCN, 15787
Oksanen A., Kehusmaa P., Harlingten C., 2014, GCN, 15786
Prochaska J. X., Chen H.-W., Bloom J. S., 2006, ApJ, 648, 95
Quadri U., Strabla L., Girelli, R., 2014, GCN, 15813
Rees M.J., Mészáros P., 1994, ApJ, 430, L93
Saito Y. et al., 2014, GCN 15803
Sonbas E., Guver T., Temiz U., Gogus E., Kocak M., Erece O., Eker Z., 2014, GCN, 15797
Spruit H.C., Daigne F., Drenkhahn G., 2001, A&A, 369, 694
Stecker F.W., 2011, Astroparticle Physics, 35, 95
Toma K. et al., 2009, ApJ, 698, 1042
Toma K. et al., 2012, Phys. Rev. D, 109, 24, 241104
Toy, V., Cenko S. B., Kutyrev A., Capone J., Troja E., Cucchiara A., Veilleux S., Gezari S., 2014, GCN, 15835
Ubertini P. et al., 2003, A&A, 411, L131
Volnova A., Stepura A., Matkin A., Molotov I., Pozanenko A., 2014, GCN, 15792
Vreeswijk P. M. et al. 2007, A&A, 468, 83
Winkler C. et al., 2003, A&A, 411, L1
Xu D., Feng G.-J., Xu J., Esamdin A., 2014, GCN, 15789
Yonetoku D. et al., 2011, ApJ, 743, L30
Yonetoku D. et al., 2012, ApJ, 758, L1
Yurkov V. et al., 2014, GCN, 15788
Zhang B. , 2014, IJMPD, 23, 30002
Zhang B., Huirong Y. al., 2011, ApJ, 726, 90